1D-3D coupled approach for the evaluation of the in-cylinder conditions for Gasoline Compression Ignition Combustion

1D-3D coupled approach for the evaluation of the in-cylinder conditions for Gasoline Compression Ignition Combustion

Davide Viscione, Gian Marco Bianchi, Vittorio Ravaglioli, Stefania Falfari, Giulio Cazzoli, Giacomo Silvagni, Valerio Mariani, Marzia Corsi

DIN – Dipartimento di Ingegneria Industriale, Alma Mater Studiorum – Università di Bologna, Bologna, 40121 Italy

davide.viscione2@unibo.it; gianmarco.bianchi@unibo.it; vittorio.ravaglioli2@unibo.it; stefania.falfari@unibo.it; giulio.cazzoli@unibo.it; giacomo.silvagni2@unibo.it; valerio.mariani4@unibo.it; marzia.corsi2@unibo.it

Abstract. Nowadays, progressive improvements of engine performance must be performed to reduce fuel consumption, which directly affects the amount of CO2 released in the atmosphere. For this purpose, considering modern technologies in the automotive scenario, Gasoline Compression Ignition (GCI) combustion might represent one promising solution, since it experiences high thermal efficiency of Compression Ignited (CI) engines and pollutant emission mitigation. This paper shows the first step of a project aimed at reproducing the combustion behavior of a Diesel engine running with GCI combustion by means of CFD simulations. In particular, this work presents a methodology used to reconstruct the mixing process inside the cylinder before the combustion event, since those engines are dramatically sensitive to the global and local mixture quality. Firstly, a reverse-engineering procedure aimed at generating the CAD model of the engine was performed. Afterwards, the discharge coefficients of the intake and exhaust valves through specifically designed 3D CFD simulations were determined, which was necessary due to the customized intake/exhaust line. Eventually, to reasonably reconstruct the in-cylinder state, the Rate of Heat Release (RoHR) curve, calculated from the analysis of the in-cylinder pressure signal running the engine in GCI mode, was imposed in GT-Power by means of a combination of Wiebe functions with the purpose of generating representative trends of pressure, temperature, and mass flow to properly define the domains of the CFD model.

1. Introduction

During the last decades, the increasingly stringent limits on the pollutants emitted by a vehicle have pushed the automotive industry to design more clean and efficient powertrains. The introduction of new technologies for turbocharging [1], direct injection in downsized spark-ignition engines [2, 3] and knock mitigation [4, 5] has been effective for the improvement of engine performance in terms of efficiency and pollutants released in the atmosphere and it is currently one the most common solution adopted by Original Equipment Manufacturers (OEMs) together with electrification. It is also well known that the achievement of the simultaneous reduction of all the main pollutants in light-duty conventional combustions systems, Particulate Matter (PM), Nitrogen Oxides (NOx), Unburn Hydrocarbons (UHC) and Carbon Monoxide (CO), throughout the operative engine map, is quite

challenging, especially considering the current homologation procedures. This is mainly the reason why researchers in the automotive field have recently focused their studies also on the development of innovative combustion processes. In this framework, Low-Temperature Combustion (LTC) systems combine the features of both the Spark-Ignition and Compression-Ignition combustions. Combustion chamber geometry, air-flow path, spray pattern and injection strategy have been optimized for those combustions to obtain an overall reduced temperature, a greater efficiency during the combustion process [6] and thus, lower pollutants emissions at the engine tailpipe.

Although these new concepts have the potential to reduce or even eliminate the after-treatment systems for PM an NOx, their most critical aspects are the combustion control and the operative range in terms of output load [7]. In fact, the combustion phasing is strongly affected by the intake air thermodynamic conditions. For this reason, in order to extract the highest indicated efficiency, a huge effort on developing complex control algorithms which relate the combustion indexes and the thermodynamic state is necessary. Moreover, LTCs suffer from limited operability in the engine map. At very low-load conditions, the in-cylinder pressure and temperature may not sustain the combustion, leading to quite high Coefficient of Variation (COV) for the Indicated Mean Effective Pressure (IMEP), with concerns on stability and repeatability of the combustion process. Conversely, during high-load conditions, the combustion process may be very sharp, with concerns on the lifetime and the reliability of some engine components. Those limits can be clearly understood in the analysis of the benchmark of LTCs, the Homogeneous-Charge Compression Ignition (HCCI) [8], in which a premixed gasoline-like mixture is introduced inside a high-compression ignition engine, auto igniting almost simultaneously. Overlapping the operating points investigated during the current homologation procedures and the ones covered by a HCCI combustion, the latter cannot provide a significant improvement on the engine performance because of its narrow applicability, thus other LTCs have been developed to enlarge this region.

In a Gasoline Compression Ignition (GCI) combustion, a gasoline-like fuel is injected in multiple late injections (MLI) creating a stratified charge [9]. Compared to conventional Diesel engine's performances, the GCI combustion has shown lower values for Indicated Specific Fuel Consumption (ISFC), Indicated Specific Nitrous Oxides emissions (ISNOx) and Filter Smoke Number (FSN) [10] at almost all the engine operations investigated. For these reasons, the GCI combustion mode is worth to be investigated. MLIs significantly improve the combustion phase control, since the energy released is directly dependent on the injection strategy and spray pattern. Similarly to Conventional Diesel Engines (CDE), the first injections are crucial for the realization of efficient and repeatable combustions, thus a deeper knowledge on the ignition delay of gasoline at GCI-like conditions is necessary [11, 12].

In the literature there are several articles related to the study of GCI combustion with the integration of CFD methodology. A parametric study about the impact of fuel injection strategy and boundary condition has been conducted in [13] in order to investigate the combustion process and pollutant emissions in a light duty Diesel engine operating with GCI combustion. Once the model has been validated comparing CFD and experimental results in terms of in-cylinder pressure, the injection pattern and boundary conditions have been modified to account their effect. The simulations show that increasing the temperature of the intake air leads to a reduction of the ignition delay due to the improved chemical reaction rate. Moreover, a split injection strategy is beneficial for the reduction of the Maximum Peak Pressure Rate (MPPR) and of all the pollutants. At last, also the injection pressure has been investigated. The latter parameter is beneficial up to a critical value, above which the combustion hinders. The reference article [14] reports a study on the mixture formation and charge distribution given by the variation of Swirl Ratio (SR) in a CDE converted to work in GCI mode. The adoption of a different fuel leads to a completely different charge distribution inside the combustion chamber. In fact, unlike for Diesel sprays, for which fuel distribution is also affected by the combustion chamber shape, gasoline fuel remains trapped in the central region due to the higher evaporation rate. According to different values of Swirl Ratio (SR), the engine releases a different amount of UHC. In fact, due to the over-mixing provided by greater SR's, the flame is not able to

propagate in the peripherals. On the other hand, for lower values of SR, richer pockets are generated in the central piston bowl region, leading to a sharper heat release rate. For those reasons, a different geometry for the piston might be effective for the reduction of UHC emissions and for the mitigation of the heat release rise rate. The latter geometrical consideration is studied in deep in [15], in which a different piston bowl design with respect to the baseline configuration produces lower amounts of pollutants during high load operations. This is due to a better distribution of the fuel vapour, leading to a reduced presence of richer pockets. In fact, especially in the late combustion phase, the mass fraction of lean charge is higher with respect to the baseline configuration, owing to a reduced amount of UHC, PM and CO emissions.

A precise calibration of the CFD model with experimental data is useful during the optimization phase of the design process. By performing parametric studies in the CFD environment, it is possible to get suggestions regarding strategies to reduce the pollutants released and to increase the engine efficiency without having the cost that equivalent experiments must consider.

This work, based on a large collection of experimental data on the GCI engine test bench placed in the laboratory of Forlì [16, 17], gives an overview of the numerical methodology adopted to investigate the mixing process occurring inside that engine system, with the aim to provide insights on the effectiveness of the adopted injection strategy to promote a correct mixture 3D distribution. This task plays a key role since the only alternative way of achieving this information, is the use of optical analyses. The determination of the discharge coefficients of the valves has been effective to validate the air flow path in terms of trapped mass inside the cylinder at Intake Valve Closing (IVC). Concerning the spray characterization, results are in good agreement with experiments regarding the overall mixture composition and local stratification. Considering that the spray break-up and wall interaction models have not been optimized for the current injector, further studies have the potential to improve the results.

2. Methodology

The work presented in this article represents the preliminary part of a project aimed at validating and optimizing the GCI combustion starting from data provided by experiments at the test bench. For this reason, the whole computational environment has been defined from scratch. A representative scheme of the procedure is highlighted Figure 1.

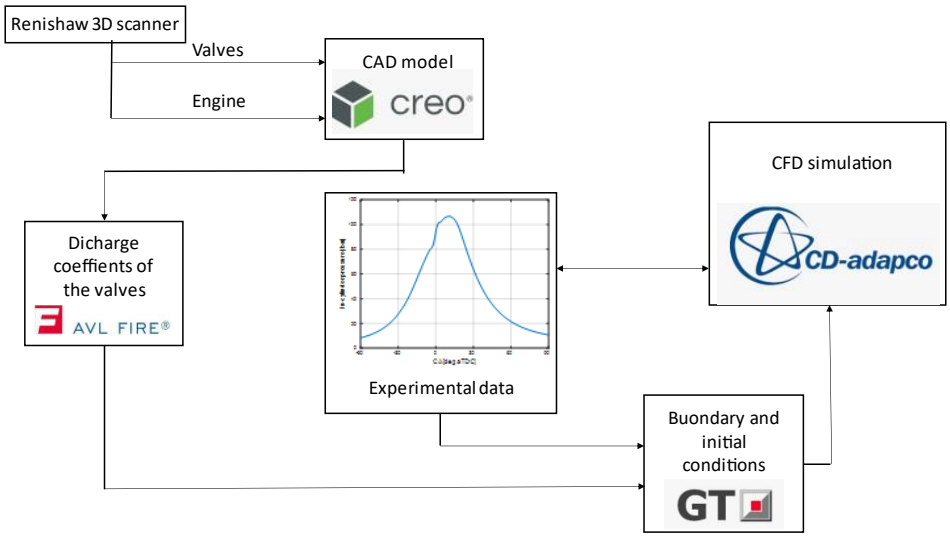

Figure 1: scheme of the procedure

2.1. Development of the CAD model of the engine

For the preliminary development of a 3D-CFD methodology of the GCI engine, the CAD model of the combustion chamber and of the intake and exhaust ports and valves of the engine have been reconstructed directly inside the Engineering department. The characteristics of the engine can be found below in the Table 1.

Table 1: engine technical characteristics

Displaced volume	1248 cc
Maximum torque	200 Nm at 1500 rpm
Maximum power	70 kW at 3800 rpm
Bore x Stroke	69.6 x 82.0 mm
Compression ratio	16.8:1
Number of valves	4 per cylinder
Architecture	L4
Injection system	Common Rail, Multi-jet
Number of nozzles	7
Spray angle	150°

A Renishaw 3D scanner has been used to obtain the STL file of each half geometry of the engine components. The latter have been post-processed to obtain the whole connected computational volume. An explementary illustration of how the 3D scanner works can be seen in Figure 2 (a) and figure 2 (b), which show the intake valve and its respective STL file.

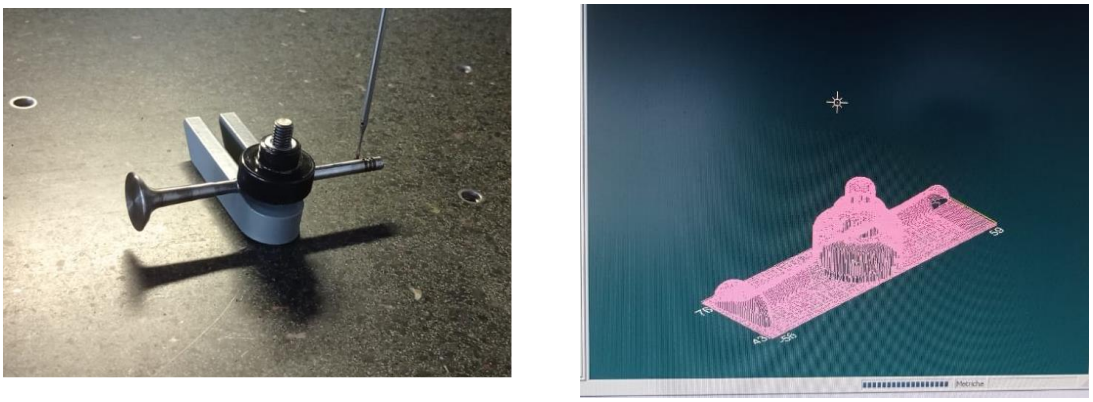

Figure 2: (a) scanned intake valve; (b) resulting STL file

All the scanned geometries have been post-processed and connected in the CAD environment Creo Parametric. The volume is then imported in the software STAR-CCM+ for the pre-meshing operations. The resulting geometry of the engine can be seen in Figure 3. At this point, all the boundary faces are attributed with their respective names, because it will be beneficial for a faster meshing operation later. Moreover, in STAR-CCM+ the edges of the mesh can be chosen arbitrarily. Then, the software performs a surface meshing which includes the local refinements.

The intake and the exhaust ports have a specific shape, as it can be seen in figure 3. In fact, since the engine has been designed to work with Diesel combustion, one of the two intake ports is denoted as the “Swirl port” (pink duct), since it is meant to generate the Swirl vortex.

In order to produce precise results from CFD simulations, proper boundary and initial conditions must be set. The latter are generated using the one-dimensional code GT-Power, which is meant to reproduce the in-cylinder conditions in the engine accurate as well.

Since the GCI combustion is strongly dependent on the charge distribution inside the combustion chamber, the behavior of the mass flow through the intake valves must be as accurate as possible.

Thus, preliminary steady-state CFD simulations with the commercial software AVL Fire have been performed in order to calculate the proper discharge coefficients of the valves.

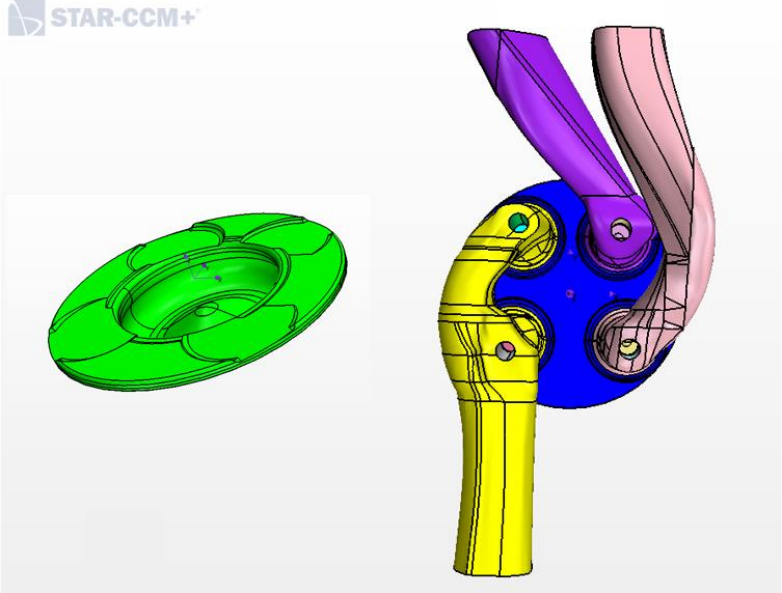

Figure 3: CAD of the engine and piston in STAR-CCM+

2.2. Determination of the discharge coefficients of the valves

2.2.1. Theoretical background

The valve discharge coefficient curves represent the fluid dynamic efficiency of the engine [18]. In fact, they are the ratio between the actual air flow and the one calculated by isentropic relations, as equation 1 states [19]:

$$\dot{m}_{theoretical} = \frac{A_{ref} p_0}{\sqrt{RT_0}} \sqrt{\frac{2\gamma}{\gamma - 1}\left(\beta^{\frac{2}{\gamma}} - \beta^{\frac{\gamma+1}{\gamma}}\right)} \quad (1)$$

for which p_0 and T_0 represent the total pressure and temperature before the valves, R and γ are the specific gas constant and heat capacity ratio of air and β is the pressure ratio between upstream and downstream the valve. A_{ref} could be the valve curtain area, which changes according to the actual valve lift, or it could be the valve seat area. Depending on which one of the two reference area is taken, the discharge or flow coefficient is calculated, respectively. In the present study only the valve seat area has been taken into consideration.

2.2.2. Generation of the curves for the flow coefficients

Figure 4 shows an example of the imported STL file for the computational domain in AVL Fire.

The computational domain has been modified to properly calculate the flow coefficients. In fact, the ports and the cylinder have been lengthened to ensure a fully developed flow [18, 20]. Moreover, before entering the ports the flow passes through a bigger volume, which approximates the calm region (pink volume in Figure 4). The flow coefficients have been calculated separately for intake and exhaust valves. Thus, while the coefficients have been computed for the intake valves, the exhaust port and valves have been disregarded from the domain to reduce the computational time.

To reduce the influence of the stroke length in the overall mass flow though the valves, the stroke has been lengthened up to 5 times its value. A calm volume, whose diameter has been fixed at 4 times

the inlet one, has been added to the domain to stabilize the in-flow. Moreover, the piston has been removed from the geometry and it has been substituted with an inlet/outlet section. In fact, between the calm volume and the fictious piston a constant pressure difference has been imposed to guide the flow in the desired direction. The complete computational volume can be seen in Figure 4 (a). The maximum cell size has been set to 6 mm. Local refinements have been performed to improve the accuracy of the results. The latter are highlighted in Figure 4 (b) for the valve plate and valve seat, for which the minimum cell size has been imposed to 0.75 mm. Depending on the actual valve lift the number of boundary layers has been imposed from 4 to 6. The resulting number of cell lays between 4 and 5 million.

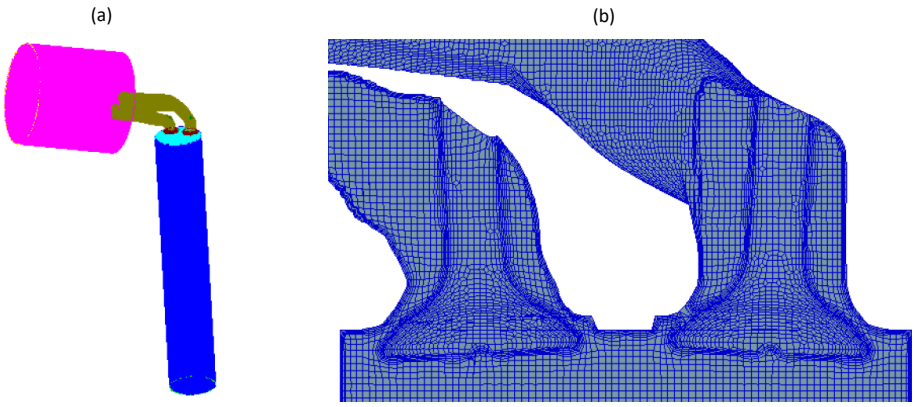

Figure 4: (a) modified computational domain for the calculation of flow coefficients for the exhaust valves; (b) local refinements on the valve plate and seat

Simulations have been performed at steady-state conditions, with the wall temperature fixed at 298 K. The real mass flow has been computed with five different lifts: 1, 2, 4, 6 and 8 mm. Inlet total pressure and outlet static pressure have been imposed at 1 bar and 0.89 bar, respectively. The turbulence model was set to k-zeta-f.

Results of the simulations can be seen in Figure 5. It is interesting to underline that, once the valve lift reaches values above 4 mm, the increment in trapped mass approaches a stable value. This is due to different flow regimes. In fact, while the valve lift increases, the valve curtain area increases accordingly, owing the flow to separate from the valve plate and head. The latter consideration can be also understood by analysing the velocity magnitude field in a plane crossing the valves, as highlighted in Figure 6 for valve lift of 2 mm and 8 mm respectably. For the highest valve lift, most of the mass flow is introduced in the region between the head and the left side of the valve, while, for the right one, the flow is almost settled. This is given by the flow separation occurring in the head side. For the lower valve lift, the latter phenomenon is much less pronounced since it can be seen only in the valve on the left of the Figure 6 (a).

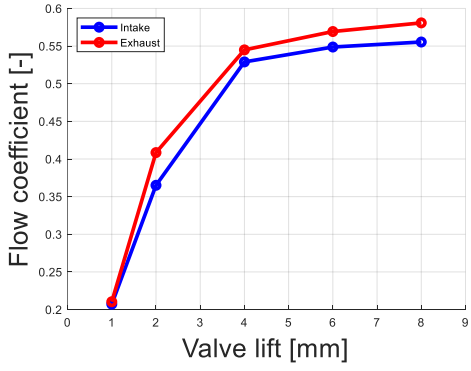

Figure 5: Comparison between flow and discharge coefficients

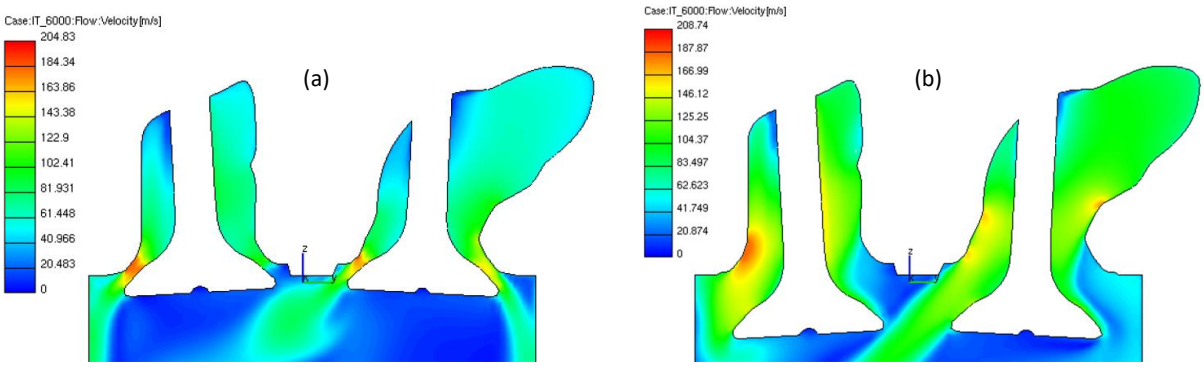

Figure 6: (a) velocity field at 2 mm intake valve lift; (b) velocity field at 2 mm intake valve lift

The coefficients shown in figure 6 have been exported in the one-dimensional code GT-Power to reconstruct the boundary and initial conditions to impose in the 3-D CFD simulations.

2.3. Determination of the boundary conditions

The one-dimensional code GT-Power is a powerful tool which simulates the gas dynamics in an internal combustion engine. It requires inputs such as the environmental thermodynamic conditions, the mass composition, the valve lifts, the discharge coefficients and the RoHR curve and it delivers the behaviour of one or more desired quantity during the engine cycle. In particular, the RoHR curve is reconstructed by means of a linear combination on Wiebe functions [21], which are obtained by a fitting algorithm in MATLAB. By analysing the experimental data, the fitting algorithm reconstruct the experimental RoHR trace by means of three Wiebe functions, for which two of them are meant to represent the premixed part of the combustion, while the last one acts as the diffusive combustion process. The reference experimental RoHR curve and the resulting fitting Wiebe functions are shown in Figure 7.

Since the gasoline fuel experiences a longer ignition delay compared to Diesel, it is necessary to increase pressure and temperature inside the cylinder to promote the fuel oxidation. Thus, two consecutive short injection pulses before the main injection are beneficial for the pressure and temperature increase. In fact, the fuel injected in the early injections leads to an almost premixed and fast combustion, as shown in the first stage of the RoHR curve in Figure 7. In this way, the ignition delay related to the Main injection is much more reduced, leading to a better control capability of the combustion phasing. The injection pressure and pattern that has been adopted to generate that RoHR curve are listed on the right of figure 7.

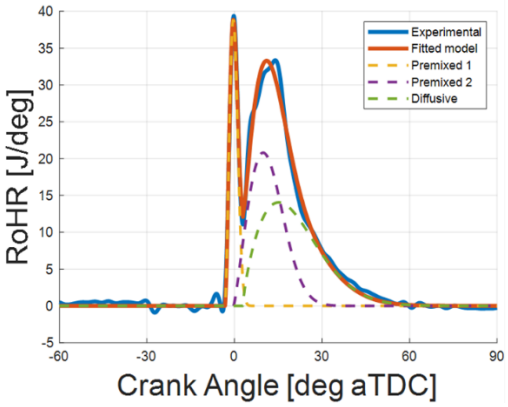

Injection pressure	600 bar
SOI Pilot, ET Pilot	35 CA bTDC, 350 μs
SOI Pre, ET Pre	21 CA bTDC, 350 μs
SOI Main, ET Main	35 CA bTDC, 350 μs
Injected fuel	22 mg

Figure 7: Experimental and fitted RoHR curve with injection pattern characterization

Since the GCI combustion is strongly dependent on mixture local conditions, a very precise calibration of the boundary and initial conditions must be performed, otherwise the mixing process

wouldn't be representative of the real experiments, resulting to a different behavior of the combustion event and the consequent in-cylinder pressure.

The RoHR in figure 8 has been chosen as the reference GCI combustion, for which the boundary and initial conditions have been derived, because it is the result of the combination of the intake air condition and injection pattern which provide a good compromise between combustion phasing controllability, performance and reliability of the engine.

By imposing the RoHR curve, the flow coefficients and the pressure and temperature conditions at the compressor outlet and turbine inlet, which have been extracted from the test bench results file, the one-dimensional model is able to provide the pressure, temperature and mass flow at the boundary sections of the engine ports.

3. Results

The validation phase has followed the comparison between the in-cylinder pressure trace given by the indicating system at the test bench and the one calculated by the CFD code. Initially, the validation focused only on the trapped mass inside the cylinder. In this way, it has been possible to state if the previous methodology was acceptable for the reconstruction of the mass flows during the engine cycle.

3.1. Air flow characterization

The CFD simulations followed the following set-up. The MARS differencing scheme has been adopted for momentum, turbulence kinetic energy and temperature with a blending factor of 0.5. For the density, the Central Differencing scheme has been chosen, with a blending factor of 0.1. The base angle step has been set to 0.1 CA (4.78*1e-4 s), but during the injection process it has been halved. The turbulence model adopted for this simulation was $k-\epsilon$ RNG.

The Figure 8 (a) shows the amount of mass in the cylinder domain during the engine cycle, with the dashed line representing the calculated air mass at the test bench.

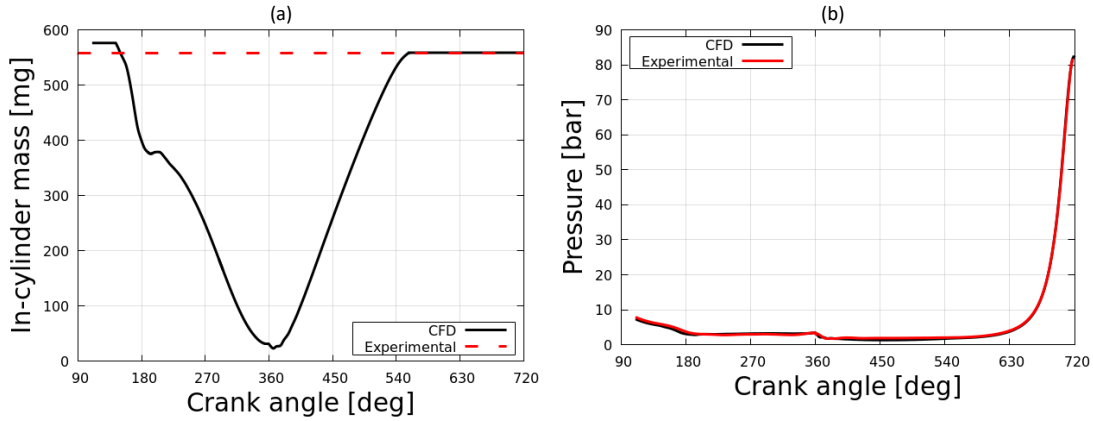

Figure 8: (a)Behaviour of the mass inside the cylinder during the engine cycle; (b) comparison between the experimental in-cylinder pressure trace and calculated

The resulted trapped mass inside the cylinder agrees with the data provided by experiments. This is also supported by looking at the Figure 8 (b), which shows the comparison between the pressure trace from the indicating system and the one calculated by the code.

Figure 9 (a) shows two noticeable coherent flow structures in an internal combustion engine: Tumble and Swirl. Tumble flow is mostly designed for SI engines to enhance fuel mixing and to provide turbulence energy in the late compression phase to speed-up the combustion. Instead, Swirl is designed in CI engines to enhance the fuel to mix with free Oxygen during the diffusive combustion process and to avoid the "cloud overlap", which is detrimental for the overall amount of pollutants released. In order to understand their evolution during the engine cycle, they are represented by the Tumble, Cross-Tumble and Swirl Ratios.

Since the engine of interest has been designed to work with CI combustion, SR is promoted against TR, as Figure 9 (a) highlights. In addition to having Tumble flow, which can be considered a collateral structure for this engine, also Cross-Tumble Ratio (CTR) can be noticed. It has the same shape of Tumble flow, but its rotational axis is rotated by 90 degrees with respect to the piston axes.

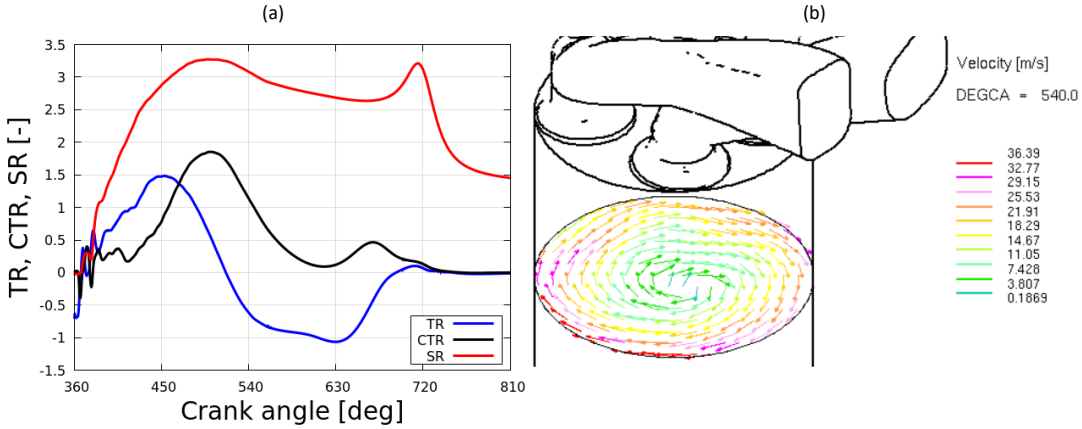

Figure 9: (a) behaviour of coherent vortexes during the engine cycle; (b) Swirl vortex at IVC

The generation of a strong Swirl flow is due to the geometry of the intake port. In fact, their geometry has been designed to direct as much as possible to a preferred direction to produce tangential flow with respect to the cylinder axis. Figure 10 gives an overview on how the geometry influences the air flow path. In Figure 10 (b) and Figure 10 (c) a strong anisotropy between the mass flows in the four curtain sections of the valves is highlighted. In Figure 10 (b) and Figure 10 (c), each mass flow refers to the one passing through the curtain sections highlighted with the same legend colour shown in Figure 10 (a). Comparing the trends in Figure 10 (b) and Figure 10 (c) it is possible to notice that both the ports participate to the generation of the Swirl flow (top valve in curtain 4 and bottom valve in curtain 3), but for the bottom valve most of the flow is directed in the tangential direction. For this reason, the bottom intake port has been denoted as “Swirl Port”. Moreover, for both the Standard and the Swirl port, a strong flow separation occurs, confirming also the results shown in Figure 5 and Figure 6. The flow in the curtain 2 of the Standard port is almost still once the valve lift reaches its maximum, owing the flow to move towards the curtains 3 and 4, for which the behaviour is almost the same. This effect is visible, but less pronounced, in the Swirl port, as the mass flow in curtain 1 suggests.

Tumble flow generation might be denoted to the combination of both the whole mass flows in the Standard and Swirl port. During the early intake phase, the introduction of air leads to the generation of a vortex rotating counterclockwise with respect to the y-axis. Instead, during the remaining intake phase, in which the Swirl flow is most generated, Tumble flow changes its rotating direction. This phenomenon probably comes from the production of Swirl flow itself, for which a collateral structure is generated too. As a result, the overall mass in the cylinder rotates around an intermediate axis between the z and y ones.

Instead, Cross-Tumble flow is generated mostly by the Flow port, in which the mass flows passing though the curtains 3 and 4 are almost the same, owing to the realization of a vortex rotating around the x-axis. During the late compression phase, both the Tumble flows are reduced in favour of Swirl flow, as the SR increment around TDC suggests.

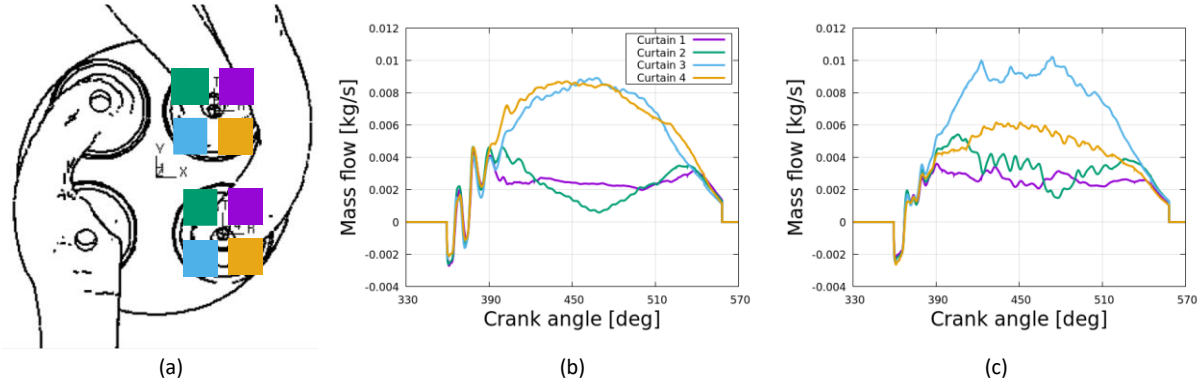

Figure 10: (a) Division of the intake valves curtain sections; (b) mass flows at the Standard port valve; (c) mass flows at the Swirl port valve.

Since the Swirl flow increases in the late compression phase due to the energy supplied the two Tumble vortexes, the resulting Turbulence Kinetic Energy (TKE) available in the combustion chamber is poor. The amount of TKE is computed by the non-dimensional term u', which relates the velocity of the turbulent flow with respect to the mean piston velocity:

$$u' = \frac{\sqrt{\frac{2}{3}TKE}}{2cn} \tag{2}$$

During the late compression phase, u' starts increasing due to the reduction of Swirl and Cross-Tumble flows. Then, it tends to be further reduced due to the Swirl flow intensity increase. The Figure 11 (b) shows the field of u' for three consecutive crank angles, confirming that the TKE is reduced while the piston reaches the TDC.

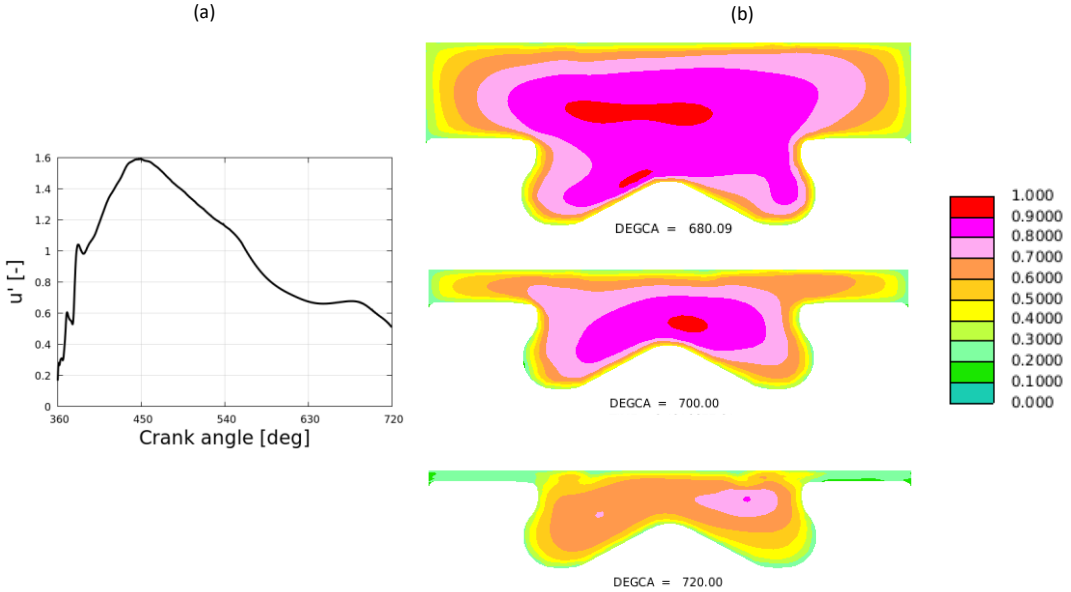

Figure 11: (a) behaviour of u' during the engine cycle, (b) 3D representation of u' in a plane perpendicular to the piston and passing thought the geometrical centre

3.2. Injection spray analysis

The current injection strategy that generates the RoHR shape in figure 8 is composed by three injection pulses. The first two of them inject a smaller amount of fuel, while the last one is meant to deliver the requested engine load. The ignition delay of the first two injections is crucial for the

stability and repeatability of the overall combustion event: the onset of the first combustion stage must be optimized in order to make the main combustion stable, repeatable and safe for the engine lifetime.

The amount of air inside the combustion chamber with respect the amount of fuel injected is denoted as Air-to-Fuel Ratio (AFR). The actual AFR is compared with a reference value, which is obtained by calculating the amount of air needed to completely oxidise 1 kg of fuel. The normalized AFR is then referred as Lambda.

Lambda influences the performance and the amount of pollutants during the combustion event. In GCI applications, it has been imposed always at leaner values (>1), meaning that the combustion operates with an excess of air, owing to a higher thermodynamic efficiency.

The Table 2 summarizes the models related to the spray-break up mechanisms.

Table 2: models for Multiphase treatment

Multi-phase	Lagrangian
Break-up model	User subroutine [22]
Droplet-wall interaction	Senda
Leidenfrost temperature	Habchi

The resulting behaviour of Lambda is highlighted in Figure 12 (b). The simulation shows a slightly lower value of Lambda with respect to the experiments, meaning that gasoline is present in the gaseous conditions in higher quantity with respect to the real case, as the Figure 12 (a) shows. The latter consideration might come from the nature of the break-up model, fuel film model or both. Further studies on the interaction between the break-up model and film model for the realization of a precise mixture will be carried out in the future based on detailed characterization of the injector. On the other hand, considering that the amount of injected fuel does not differ so much from the experiments, it is worth to quantitatively analyse the distribution of Lambda during the engine cycle events.

Figure 12 (a) compares the trends for Injected, liquid and evaporated fuel. Since the temperature inside the combustion chamber is quite high (almost 760 K at SOI Pilot), the evaporation rate is high, thus the liquid phase quickly disappears. This is even more evident for the next injections, for which the evaporation rate is even higher.

The Figure 13 (a) shows the distribution of Lambda just before the combustion onset and the injection of the Main pulse. Since the injected fuel during the first two injections is quite low, its penetration in the combustion chamber is low too. In this way, a stratified charge is generated above the piston bowl.

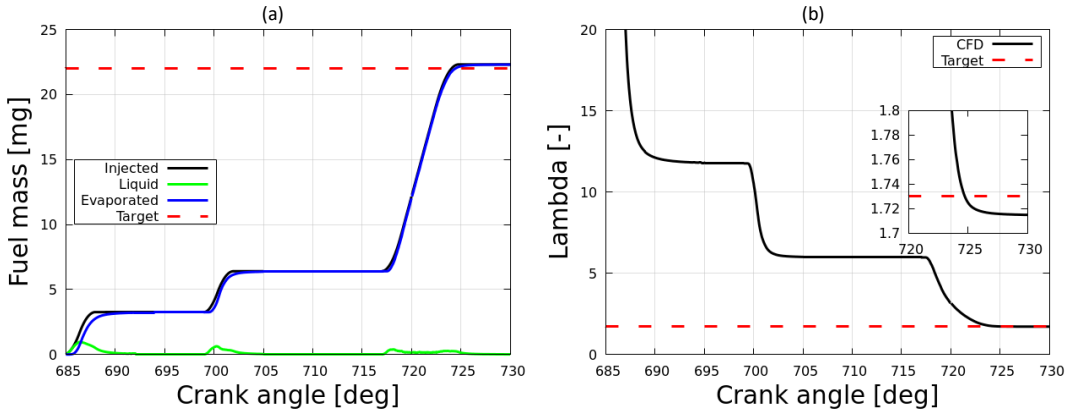

Figure 12: (a) Injected, liquid and evaporated fuel during the engine cycle; (b) behaviour of Lambda during the engine cycle

The Figure 13 (b) shows the distribution of Lambda just 1 CA after the SOI for the Main injection pulse. Thanks to the fast evaporation, it can be noticed that the additional fuel increases the area at

which the mixture is more subjected to the auto-ignition process. Hence, the ignition points could be denoted to the richer regions highlighted in the centre of the combustion chamber.

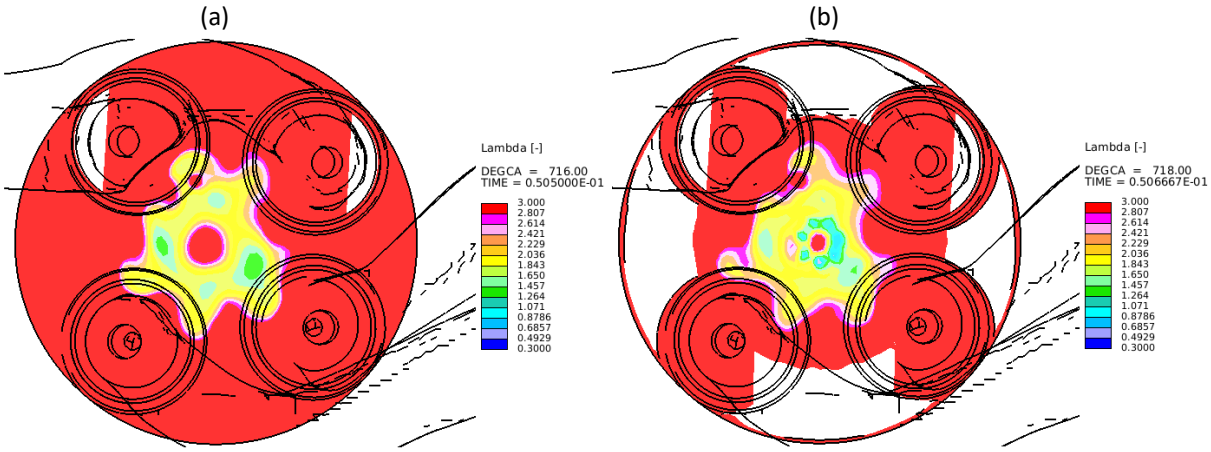

Figure 13: (a) distribution of Lambda 1 CA bSOI Main; (b) distribution of Lambda 1 CA aSOI Main

Since the first two injections provide low penetration in the combustion chamber, as the Figure 13 (a) marks, most of the fuel film might be generated during the Main injection, for which the spray protrusion is much more enhanced (Figure 14), especially in the piston bowl region. For this reason, the lower overall Lambda value might be attributed to a different behaviour of the evaporated fuel from the film itself with respect to the real case.

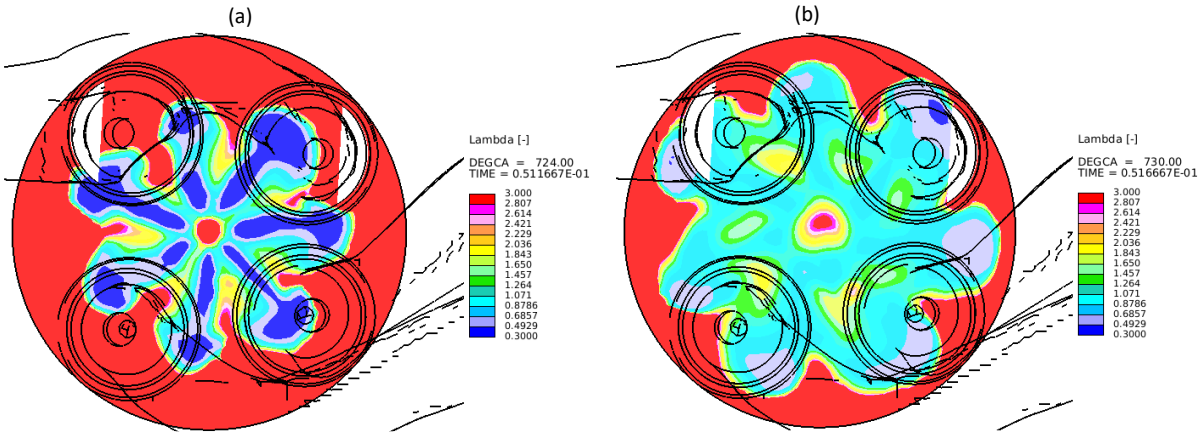

Figure 14: (a) distribution of Lambda 1 CA bEOI Main; (b) distribution of Lambda 5 CA aEOI Main

4. Summary and conclusions

In this article a numerical procedure aimed at the reconstruction of the GCI combustion starting from experimental data has been discussed. The values for the intake and exhaust discharge coefficient obtained with steady-state simulations in AVL Fire have been validated during the comparison between the real trapped mass calculated at the test bench and the same computed in Pro-STAR.

The analysis of the behaviour of the mass flows through the intake ports has been beneficial to understand the nature of the coherent vortex structures inside the cylinder. The transition of Tumble and Cross-Tumble flows to Swirl one during the late compression phase gives extra energy to the Swirl flow itself, retarding its breakdown. This is translated in a reduction of the TKE around the TDCF.

From the analysis of the spray development and the consequent mixture generation, considering the shape of the first combustion stage obtained by the in-cylinder pressure signal, the resulting field of Lambda in the combustion chamber appears to be reasonable with a mixture composition that, once

the mixture has reached the auto ignition conditions and the ignition delay has been achieved, then the combustion is triggered and a premixed combustion is realized.

Future developments on the topic of this article will be related to the comparison of the simulated combustion event with respect to the one captured at the test bench, together with the optimization of the break-up and fuel film models for a better mixture reconstruction.

References

[1] Police, G, Diana, S, Giglio, V, Iorio, B, & Rispoli, N. "Downsizing of SI Engines by Turbo-Charging." *Proceedings of the ASME 8th Biennial Conference on Engineering Systems Design and Analysis*. *Volume 4: Fatigue and Fracture, Heat Transfer, Internal Combustion Engines, Manufacturing, and Technology and Society*. Torino, Italy. July 4–7, 2006. pp. 463-476. ASME. https://doi.org/10.1115/ESDA2006-95215.

[2] Jung, D, Lee, B, Son, J, Woo, S, & Kim, Y. "Development of GDI Engine for Improving Brake Thermal Efficiency Over 44%." *Proceedings of the ASME 2019 Internal Combustion Engine Division Fall Technical Conference*. *ASME 2019 Internal Combustion Engine Division Fall Technical Conference*. Chicago, Illinois, USA. October 20–23, 2019. V001T07A004. ASME. https://doi.org/10.1115/ICEF2019-7144.

[3] Lumsden, G., OudeNijeweme, D., Fraser, N., and Blaxill, H., "Development of a Turbocharged Direct Injection Downsizing Demonstrator Engine," *SAE Int. J. Engines* 2(1):1420-1432, 2009, https://doi.org/10.4271/2009-01-1503.

[4] Ranuzzi, F., Cavina, N., Brusa, A., De Cesare, M. et al., "Development and Software in the Loop Validation of a Model-based Water Injection Combustion Controller for a GDI TC Engine," SAE Technical Paper 2019-01-1174, 2019, https://doi.org/10.4271/2019-01-1174.

[5] Ranuzzi, F., Cavina, N., Scocozza, G., Brusa, A. et al., "Experimental Validation of a Model-Based Water Injection Combustion Control System for On-Board Application," SAE Technical Paper 2019-24-0015, 2019, https://doi.org/10.4271/2019-24-0015.

[6] Sellnau, M., Hoyer, K., Moore, W., Foster, M. et al., "Advancement of GDCI Engine Technology for US 2025 CAFE and Tier 3 Emissions," SAE Technical Paper 2018-01-0901, 2018, https://doi.org/10.4271/2018-01-0901.

[7] Zhao, H., Li, J., Ma, T., and Ladommatos, N., "Performance and Analysis of a 4-Stroke Multi-Cylinder Gasoline Engine with CAI Combustion," SAE Technical Paper 2002-01-0420, 2002, https://doi.org/10.4271/2002-01-0420.

[8] Zhao, F., Asmus, T.N., Assanis, D.N., Dec, J.E. et al., Homogeneous Charge Compression Ignition (HCCI) Engines: Key Research and Development Issues (Warrendale, PA: SAE International, 2003). ISBN:978-0-7680-1123-4.

[9] Sellnau, M., Sinnamon, J., Hoyer, K., and Husted, H., "Full-Time Gasoline Direct-Injection Compression Ignition (GDCI) for High Efficiency and Low NOx and PM," *SAE Int. J. Engines* 5(2):300-314, 2012, https://doi.org/10.4271/2012-01-0384.

[10] Sellnau, M., Sinnamon, J., Hoyer, K., Kim, J. et al., "Part-Load Operation of Gasoline Direct-Injection Compression Ignition (GDCI) Engine," SAE Technical Paper 2013-01-0272, 2013, https://doi.org/10.4271/2013-01-0272.

[11] Addepalli, S., Pamminger, M., Scarcelli, R., Wang, B. et al., "Numerical Investigation of the Impact of Fuel Injection Strategies on Combustion and Performance of a Gasoline Compression Ignition Engine," SAE Technical Paper 2021-01-0404, 2021, https://doi.org/10.4271/2021-01-0404.

[12] Khaled, S., Javed, T., Farooq, A., Badra, J. at al., “Analysis of ignition temperature range and surrogate fuel requirements for GCI engine,” Fuel, Volume 312, 2022, https://doi.org/10.1016/j.fuel.2021.122978.

[13] Kim, J., Sun, H., Zhang, Y., and Li, H., "Numerical Investigation to Fuel Injection Strategy and Thermal Condition Impacts on GCI Combustion at Low and Medium Loads Using CFD," SAE Technical Paper 2021-01-1155, 2021, https://doi.org/10.4271/2021-01-1155.

[14] Ashutosh Jena, Harsimran Singh, and Avinash Kumar Agarwal , "Effect of swirl ratio on charge convection, temperature stratification, and combustion in gasoline compression ignition engine", Physics of Fluids 33, 085113 (2021) https://doi.org/10.1063/5.0059579
[15] Zhang, Y., Cho, K., and Sellnau, M., "Investigation on Combining Partially Premixed Compression Ignition and Diffusion Combustion for Gasoline Compression Ignition—Part 2: Compression Ratio and Piston Bowl Geometry Effects," *SAE J. STEEP* 2(1):59-78, 2021, https://doi.org/10.4271/13-02-01-0004.
[16] Stola, F., Ravaglioli, V., Silvagni, G., Ponti, F. et al., "Injection Pattern Investigation for Gasoline Partially Premixed Combustion Analysis," SAE Technical Paper 2019-24-0112, 2019, https://doi.org/10.4271/2019-24-0112.
[17] Stola, F., Ravaglioli, V., Silvagni, G., Ponti, F. et al., "Analysis of the Effects of Injection Pressure Variation in Gasoline Partially Premixed Combustion," SAE Technical Paper 2021-01-0517, 2021, https://doi.org/10.4271/2021-01-0517.
[18] Yang, X., Chen, Z., and Kuo, T. (May 20, 2013). "Pitfalls for Accurate Steady-State Port Flow Simulations." ASME. *J. Eng. Gas Turbines Power*. June 2013; 135(6): 061601. https://doi.org/10.1115/1.4023492
[19] Heywood, John B. Internal combustion engine fundamentals. McGraw-Hill Education, 2018.
[20] da Costa, R., Franco, R., Gomes, C., Coelho, R. et al., "Experimental Methodology and Numerical Simulation of Intake Valves Discharge Coefficients for a Single Cylinder Research Engine," SAE Technical Paper 2015-36-0267, 2015, https://doi.org/10.4271/2015-36-0267.
[21] Vibe, I. I. "Semi-empirical expression for combustion rate in engines." Proceedings of Conference on piston engines, USSR Academy of sciences, Moscow. 1956.
[22] Lucchini, T., D'Errico, G., Ettorre, D., Brusiani, F. et al., "Experimental and Numerical Investigation of High-Pressure Diesel Sprays with Multiple Injections at Engine Conditions," SAE Technical Paper 2010-01-0179, 2010, https://doi.org/10.4271/2010-01-0179.